ATLANTIC RESEARCH CORPORATION
ALEXANDRIA, VIRGINIA

TR-PL-5173-02

Improvement of the Usefulness of Pyrolytic Graphite in Rocket Motor Applications

Quarterly Progress Report
June through August, 1961

Contract No. DA-36-034-ORD-3279RD
Project No. TB4-004

Contributors:

J. D. Batchelor
S. W. McCormick
R. K. White
E. L. Olcott
E. F. Ford

September 15, 1961

Atlantic Research Corporation
Alexandria, Virginia

TABLE OF CONTENTS

I. INTRODUCTION

This report describes the work performed during the quarter from June 1, 1961 through August 31, 1961. This period begins at the completion of the first year's work which was covered in the recently published First Annual Summary Technical Report.

Emphasis has been shifted to cover rocket-motor testing of nozzles containing pyrolytic graphite coatings. Deposition studies and mechanical design studies will be continued as needed to assure the most successful performance in motor tests.

II. SUMMARY AND CONCLUSIONS

In deposition studies, the effect of the gas dynamics on the uniformity of the pyrolytic graphite deposit was noted. The process gas flow through the injector must be balanced with that outside the injector for optimum uniformity. The furnace equipment was modified to allow substrate rotation during deposition. A preliminary assessment of the effect of the substrate surface finish on the deposited coating was also made.

In the mechanical design studies, a derivation was completed for the exact stress-strain relations for a material which exhibits the form of elastic and thermal anisotropy found in pyrolytic graphite. The over-all problem of stress-strain in a cylinder of finite length was then set up. The problem was separated into two parts, one dealing with the central portion of the cylinder and other dealing with the end effects. In the first part, expressions for the stresses in a hollow cylinder of pyrolytic graphite were derived for a section removed sufficiently from the ends of the cylinder so that the edge effects were not significant. Numerical examples will be calculated for different radii and for different pyrolytic graphite thicknesses. The second part will be solved treating the edge-effect problem which is known to be closely related with coating failures. Since the thicknesses of practical coatings of pyrolytic graphite is usually small compared to its radius, a thin-wall approximation will be considered.

In the motor-firing program, a pyrolytic graphite test piece having a coarse-grained microstructure was successfully tested in a 60-second firing with Arcite 373 (5600°F) propellant. A segmented nozzle was used[1] in which the test piece was a concentric ring in the throat. The segmented test nozzle was then redesigned to use a larger, contoured section of pyrolytic graphite at the throat. Redesign was necessary for hotter firings (6500°F) since no other grade of graphite is servicable near the throat section under such demanding conditions. The substrate failed in one attempt to coat a nozzle test piece. The substrate mechanical failure was coincident with a furnace-tube failure. The furnace was repaired and further deposition tests and nozzle preparation work is under way.

III. DEPOSITION PROCESS STUDIES

The thickness and uniformity of the pyrolytic graphite coating are sensitive to the gas dynamics in the deposition zone. To prepare nozzle test pieces of the desired quality and configuration, the effect of gas dynamics, substrate geometry, and surface finish are being studied. During the period the effects of gas distribution and surface finish were investigated. A standard cylindrical substrate of one inch inside diameter was used, and all runs were made with methane as the carbon source with a total gas flow rate (methane plus diluent) of 20 SCFH.

Twelve deposition runs were made as shown in Table I. The rate of deposition of pyrolytic graphite is affected by the methane concentration. But of greater importance is the effect of gas distribution on uniformity of coating. In general, an expansion tip on the gas injector appears to improve gas distribution and the control of coating uniformity. However, in Run 34 when all the process gas entered through the injector, a heavy deposit was formed over the first four inches of the substrate with a thinner, non-uniform deposit over the remainder of the substrate. In Run 33, a non-uniform deposit was formed by passing 40 per cent of the total gas through the annulus. The non-uniformity appeared as a slightly thicker coating at the outlet end of the substrate. In Run 32, a very uniform deposit was obtained by passing 10 per cent of the total gas flow outside the injector.

Control of the uniformity of the coating in the radial direction is also important. Careful centering of the injector in the substrate tube can help produce good results. Also, provision was made to rotate the substrate relative to the injector which should allow additional control of the radial uniformity.

The surface finish of the substrate, in the range from 80 to 400 grit, does not appear to affect the coating greatly except that the finish of the coating reflects the substrate finish. The substrate surface roughness might be expected to affect the bond strength between the pyrolytic

TABLE I

CONDITIONS IN DEPOSITION PROCESS STUDIES

Run No.	Temperature (°C)	Substrate Surface Finish (grit)	Gas Injector Expansion Tip	Inert Diluent Outside Injector (per cent)	Inlet Methane Concentration (per cent)	Mean* Deposit Rate (mils/hr)
24	2000	320	Yes	10	2.5	2.5
25	2000	80	Yes	10	6	6.5
26	2000	80	Yes	10	5	6.5
27	2000	80	Yes	40	5	5.
28	2000	80	No	40	5	5.5
29	2000	80	No	40	7	7.5
30	2000	320	Yes	10	5	5.5
31	2000	400	Yes	10	5	5.
32	2000	320	Yes	10	5	5.
33	2000	320	Yes	40	5	5.5
34	2000	400	Yes	0	5	15.
35	1900	80	Yes	10	5	4.

* At cross-section where maximum thickness occurs.

graphite coating and the substrate, but this point has not been studied as yet. The mechanical design and stress analysis should provide guidance concerning the strength needed at the coating-substrate interface.

The possible advantages of deposition of pyrolytic graphite at temperatures below 2000°C justify a study of deposition at lower temperature. In the first run of the series, a failure of the heating element in the furnace and the necessary repair delayed the remaining runs. However, the furnace is now ready for operation and this study will be resumed.

IV. MECHANICAL DESIGN STUDIES

In the First Annual Summary Technical Report,[1] the effect of two moduli of elasticity (one perpendicular and one parallel to the surface) on the maximum stress in a cylinder under axisymmetric load was derived. This preliminary analysis was simplified by an assumption of plane strain which is equivalent to placing a restraint on the ends of the cylinder which does not usually exist. It now appears advantageous to make a more exact stress analysis for pyrolytic graphite shells.

An acceptable mechanical design for a pyrolytic graphite nozzle must be one in which the stresses in the nozzle do not exceed the strength of the materials. The stresses which appear in a pyrolytic graphite structure may be categorized into three groups as follows:

(1) Residual stresses produced in manufacture,

(2) Pressurization stresses produced in service, and

(3) Thermal stresses in service produced by transient temperature gradients.

The stresses in (1) above arise because of the unequal thermal contraction of pyrolytic graphite in its a-direction and c-direction during cooling from the deposition temperature. The calculation of these stresses is complicated by the elastic anisotropy of the material. The residual stresses from manufacture for a pyrolytic graphite coating on a substrate will be different from those in a free-standing shell of pyrolytic graphite, but the stresses will not vanish in either case. The stresses in groups (2) and (3) are caused by using the material in a rocket motor environment. The stresses in group (3) are expected to be significant since the low thermal conductivity of pyrolytic graphite in its c-direction leads to very large thermal gradients across the thickness of the pyrolytic graphite shell.

The following mathematical analysis represents the first phase of the attack on the stress analysis problem. Simplifying assumptions have been avoided so that general applicability can be maintained. Numerical examples will be used to illustrate the analysis when explicit solutions

become tedious. The stress analysis will be continued in an effort to treat geometries of importance for rocket motor nozzles. The work reported here appears to be of sufficient importance as ground-work to be published at this time.

A. STRESS-STRAIN RELATIONS FOR PYROLYTIC GRAPHITE

Pyrolytic graphite, which exhibits a limited form of anisotropy, is better described as a "transversely isotropic" material, i.e., all directions parallel to the deposit plane are elastically equivalent. It can be shown[2] that the energy stored per unit volume of such a material is given in terms of the local strains by an expression involving five independent constants. Taking a rectangular coordinate system with the y-axis perpendicular to the deposit plant, this "strain-energy function" may be written as

$$W = \frac{C_{11}}{2}(\epsilon_x^2 + \epsilon_z^2) + \frac{C_{22}}{2}\epsilon_y^2 + C_{12}(\epsilon_x\epsilon_y + \epsilon_y\epsilon_z)$$

$$+ C_{13}\epsilon_x\epsilon_z + \frac{C_{44}}{2}(\gamma_{xy}^2 + \gamma_{yz}^2) + \frac{C_{11} - C_{13}}{4}\gamma_{zx}^2 \qquad (1)$$

where the C's are constants, the ϵ's are normal strains, and the γ's are shear strains. The nomenclature is standard engineering notation such as that described by Timoshenko.[3] The stress-strain relations for such a material may be found from (1) by partial differentiation:

$$\frac{\partial W}{\partial \epsilon_x} = \sigma_x = C_{11}\epsilon_x + C_{12}\epsilon_y + C_{13}\epsilon_z \qquad (2.1)$$

$$\frac{\partial W}{\partial \epsilon_y} = \sigma_y = C_{12}\epsilon_x + C_{22}\epsilon_y + C_{12}\epsilon_z \qquad (2.2)$$

$$\frac{\partial W}{\partial \epsilon_z} = \sigma_z = C_{13}\epsilon_x + C_{12}\epsilon_y + C_{11}\epsilon_z \qquad (2.3)$$

$$\frac{\partial W}{\partial \gamma_{xy}} = \tau_{xy} = C_{44}\gamma_{xy} \qquad (2.4)$$

$$\frac{\partial W}{\partial \gamma_{yz}} = \tau_{yz} = C_{44}\gamma_{yz} \tag{2.5}$$

$$\frac{\partial W}{\partial \gamma_{zx}} = \tau_{zx} = \frac{C_{11} - C_{13}}{2}\gamma_{zx} \tag{2.6}$$

where the σ's are normal stresses and the τ's are shear stresses.

The strain-stress relations may also be written in terms of seven "engineering" elastic moduli:

$$\epsilon_x = \frac{1}{E_{\parallel}}\sigma_x - \frac{\nu_1}{E_{\perp}}\sigma_y - \frac{\nu_3}{E_{\parallel}}\sigma_z \tag{3.1}$$

$$\epsilon_y = -\frac{\nu_2}{E_{\parallel}}\sigma_x + \frac{1}{E_{\perp}}\sigma_y - \frac{\nu_2}{E_{\parallel}}\sigma_z \tag{3.2}$$

$$\epsilon_z = -\frac{\nu_3}{E_{\parallel}}\sigma_x - \frac{\nu_1}{E_{\perp}}\sigma_y + \frac{1}{E_{\parallel}}\sigma_z \tag{3.3}$$

$$\gamma_{xy} = \frac{\tau_{xy}}{G_{\perp}} \tag{3.4}$$

$$\gamma_{yz} = \frac{\tau_{yz}}{G_{\perp}} \tag{3.5}$$

$$\gamma_{zx} = \frac{\tau_{zx}}{G_{\parallel}} \tag{3.6}$$

where the ν's are Poisson's ratios, the E's are Young's moduli, and the G's are moduli of rigidity. The subscript $\parallel$ refers to the plane parallel to the coating surface (a-direction in pyrolytic graphite terminology); the subscript $\perp$ refers to the axis perpendicular to the coating surface (c-direction). Only five of the engineering moduli are independent, since it can be deduced from the equations (2) that

$$\frac{\nu_1}{E_{\perp}} = \frac{\nu_2}{E_{\parallel}} \tag{4.1}$$

$$G_{\parallel} = \frac{E_{\parallel}}{2(1 + \nu_3)} \tag{4.2}$$

The engineering moduli are given in terms of the C's by the relations

$$E_{\parallel} = (C_{11} - C_{13})\left(1 + \frac{C_{13}C_{22} - C_{12}^2}{C_{11}C_{22} - C_{12}^2}\right) \tag{5.1}$$

$$E_{\perp} = C_{22} - 2\frac{C_{12}^2}{C_{11} + C_{13}} \tag{5.2}$$

$$\nu_1 = \frac{C_{12}}{C_{11} + C_{13}} \tag{5.3}$$

$$\nu_2 = \frac{C_{12}(C_{11} - C_{13})}{C_{11}C_{22} - C_{12}^2} \tag{5.4}$$

$$\nu_3 = \frac{C_{13}C_{22} - C_{12}^2}{C_{11}C_{22} - C_{12}^2} \tag{5.5}$$

$$G_{\parallel} = \frac{C_{11} - C_{13}}{2} \tag{5.6}$$

$$G_{\perp} = C_{44} \tag{5.7}$$

The C's are given in terms of the engineering moduli by

$$C_{11} = \frac{E_{\parallel}}{1 + \nu_3}\ \frac{1 - \nu_1\nu_2}{1 - 2\nu_1\nu_2 - \nu_3} \tag{6.1}$$

$$C_{12} = \frac{\nu_1 E_{\parallel}}{1 - 2\nu_1\nu_2 - \nu_3} \tag{6.2}$$

$$C_{13} = \frac{E_{\parallel}}{1 + \nu_3}\ \frac{\nu_1\nu_2 + \nu_3}{1 - 2\nu_1\nu_2 - \nu_3} \tag{6.3}$$

$$C_{22} = \frac{\nu_1 (1 - \nu_3) E_{\parallel}}{\nu_2 (1 - 2\nu_1\nu_2 - \nu_3)} \tag{6.4}$$

$$C_{44} = C_{\perp} \tag{6.5}$$

The condition that the strain-energy function (1) must always be positive or zero leads to a set of inequalities which must be satisfied by the C's:

$$C_{11} \geq 0 \tag{7.1}$$

$$C_{11} \geq C_{13} \geq - C_{11} \tag{7.2}$$

$$C_{22}(C_{11} + C_{13}) - 2C_{12}^{2} \geq 0 \tag{7.3}$$

$$C_{44} \geq 0 \tag{7.4}$$

The corresponding inequalities for the engineering modul are

$$E_{\parallel} \geq 0 \tag{8.1}$$

$$E_{\perp} \geq 0 \tag{8.2}$$

$$G_{\parallel} \geq 0 \tag{8.3}$$

$$G_{\perp} \geq 0 \tag{8.4}$$

$$1 \geq \nu_3 \geq - 1 \tag{8.5}$$

$$1 - 2\nu_1\nu_2 - \nu_3 \geq 0 \tag{8.6}$$

If thermal expansion effects are important, the equations (3) must be rewritten as

$$\epsilon_x = \frac{\sigma_x}{E_{\parallel}} - \frac{\nu_1}{E_{\perp}} \sigma_y - \frac{\nu_3}{E_{\parallel}} \sigma_z + A_{\parallel}(T) \tag{9.1}$$

$$\epsilon_y = -\frac{\nu_2}{E_{\parallel}}\sigma_x + \frac{\sigma_y}{E_{\perp}} - \frac{\nu_2}{E_{\parallel}}\sigma_z + A_{\perp}(T) \tag{9.2}$$

$$\epsilon_z = -\frac{\nu_3}{E_{\parallel}}\sigma_x - \frac{\nu_1}{E_{\perp}}\sigma_y + \frac{\sigma_z}{E_{\parallel}} + A_{\parallel}(T) \tag{9.3}$$

$$\gamma_{xy} = \frac{\tau_{xy}}{G_{\perp}} \tag{9.4}$$

$$\gamma_{yz} = \frac{\tau_{yz}}{G_{\perp}} \tag{9.5}$$

$$\gamma_{zx} = \frac{\tau_{zx}}{G_{\parallel}} \tag{9.6}$$

$$\text{where } A_{\parallel}(T) = \int_{T_o}^{T} \alpha_{\parallel}(T)\, dT, \tag{10.1}$$

$$A_{\perp}(T) = \int_{T_o}^{T} \alpha_{\perp}(T)\, dT. \tag{10.2}$$

Here $\alpha_{\parallel}$ and $\alpha_{\perp}$ are the thermal expansion coefficients of the material in directions respectively parallel to, and perpendicular to the deposit plane.

In the case of pyrolytic graphite, "T_o" must be interpreted as a temperature at which the material is free of internal thermal stresses, e.g. the deposition temperature.

When the equations (3) are similarly modified to include the effects of thermal expansion, the results are

$$\sigma_x = C_{11}\epsilon_x + C_{12}\epsilon_y + C_{13}\epsilon_z - B_1(T) \tag{11.1}$$

$$\sigma_y = C_{12}\epsilon_x = C_{22}\epsilon_y + C_{12}\epsilon_z - B_2(T) \tag{11.2}$$

$$\sigma_z = C_{13}\epsilon_x + C_{12}\epsilon_y + C_{11}\epsilon_z - B_1(T) \tag{11.3}$$

$$\tau_{xy} = C_{44}\gamma_{xy} \tag{11.4}$$

$$\tau_{yz} = C_{44}\gamma_{yz} \tag{11.5}$$

$$\tau_{zx} = \frac{C_{11} - C_{13}}{2}\gamma_{zx} \tag{11.6}$$

where

$$B_1(T) = (C_{11} + C_{13})A_{\parallel}(T) + C_{12}A_{\perp}(T) \tag{12.1}$$

$$B_2(T) = 2C_{12}A_{\parallel}(T) + C_{22}A_{\perp}(T) \tag{12.2}$$

B. STRESSES IN A HOLLOW CYLINDER OF PYROLYTIC GRAPHITE

The stress-strain relations derived above (Equations 11) must be converted to the cylindrical coordinate system (r, θ, z). Since pyrolytic graphite coatings form with the layer planes (a-direction) parallel to the substrate surface, the axis of elastic symmetry (c-direction) of the pyrolytic graphite is radially directed. In cylindrical coordinates the equations (11) become:

$$\sigma_\theta = C_{11}\epsilon_\theta + C_{12}\epsilon_r + C_{13}\epsilon_z - B_1(T) \tag{13.1}$$

$$\sigma_r = C_{12}\epsilon_\theta + C_{22}\epsilon_r + C_{12}\epsilon_z - B_2(T) \tag{13.2}$$

$$\sigma_z = C_{13}\epsilon_\theta + C_{12}\epsilon_r + C_{11}\epsilon_z - B_1(T) \tag{13.3}$$

$$\tau_{r\theta} = C_{44}\gamma_{r\theta} \tag{13.4}$$

$$\tau_{rz} = C_{44}\gamma_{rz} \tag{13.5}$$

$$\tau_{\theta z} = \frac{C_{11} - C_{13}}{2}\gamma_{\theta z} \tag{13.6}$$

The cylinder is assumed to be of finte length 2L; the ends at $z = \pm L$ are free to move.

We will consider those stresses which arise from pressurization, unequal thermal expansion coefficients, and radial temperature

gradients. In all these cases the elastic deformation is axisymmetric, and the shearing strains $\gamma_{r\theta}$, $\gamma_{\theta z}$ vanish. From (13.4) and (13.6), the shearing stresses $\tau_{r\theta}$ and $\tau_{\theta z}$ must vanish also.

The equations of elastic equilibrium reduce to

$$\frac{\partial \sigma_r}{\partial r} + \frac{\partial \tau_{rz}}{\partial z} + \frac{\sigma_r - \sigma_\theta}{r} = 0 \tag{14.1}$$

$$\frac{\partial \tau_{rz}}{\partial r} + \frac{\partial \sigma_z}{\partial z} + \frac{\tau_{rz}}{r} = 0 \tag{14.2}$$

Now let u, v, W be the displacements of the strained elastic material parallel to the r, θ, and Z axes, respectively. Because of the axisymmetric nature of this problem, v = o. The strains ϵ_r, ϵ_θ, ϵ_z, γ_{rz} are connected with the displacements u, W, by the equations

$$\epsilon_r = \frac{\partial u}{\partial r} \tag{15.1}$$

$$\epsilon_\theta = \frac{u}{r} \tag{15.2}$$

$$\epsilon_z = \frac{\partial W}{\partial z} \tag{15.3}$$

$$\gamma_{rz} = \frac{\partial u}{\partial z} + \frac{\partial W}{\partial r} \tag{15.4}$$

By using the stress-strain equations (13), the stresses can be expressed in terms of the displacements as

$$\sigma_\theta = C_{11}\frac{u}{r} + C_{12}\frac{\partial u}{\partial r} + C_{13}\frac{\partial W}{\partial z} - B_1(r) \tag{16.1}$$

$$\sigma_r = C_{12}\frac{u}{r} + C_{22}\frac{\partial u}{\partial r} + C_{12}\frac{\partial W}{\partial z} - B_2(r) \tag{16.2}$$

$$\sigma_z = C_{13}\frac{u}{r} + C_{12}\frac{\partial u}{\partial r} + C_{11}\frac{\partial W}{\partial z} - B_1(r) \tag{16.3}$$

$$\tau_{rz} = C_{44}\left(\frac{\partial u}{\partial z} + \frac{\partial W}{\partial r}\right) \tag{16.4}$$

(Here $B_1(r)$ and $B_2(r)$ have been written instead of $B_1[T(r)]$ and $B_2[T(r)]$.) Putting these relations into the equilibrium equations (14), we find

$$C_{22}\left(\frac{\partial^2 u}{\partial r^2} + \frac{1}{r}\frac{\partial u}{\partial r}\right) + C_{44}\frac{\partial^2 u}{\partial z^2} + (C_{12} + C_{44})\frac{\partial^2 W}{\partial r \partial z} - C_{11}\frac{u}{r^2}$$

$$+ (C_{12} - C_{13})\frac{1}{r}\frac{\partial W}{\partial z} = \frac{B_2 - B_1}{r} + \frac{\partial B_2}{\partial r} \tag{17.1}$$

and

$$(C_{12} + C_{44})\frac{\partial^2 u}{\partial r \partial z} + (C_{13} + C_{44})\frac{1}{r}\frac{\partial u}{\partial z} + C_{44}\left(\frac{\partial^2 W}{\partial r^2} + \frac{1}{r}\frac{\partial W}{\partial r}\right)$$

$$+ C_{11}\frac{\partial^2 W}{\partial z^2} = 0 \tag{17.2}$$

We must solve the equations (17.1) and (17.2) with the boundary conditions

$$\sigma_r = P_i,\ \tau_{rz} = 0 \qquad \text{at} \qquad r = R_i$$

$$\sigma_r = P_o,\ \tau_{rz} = 0 \qquad \text{at} \qquad r = R_o$$

$$\sigma_z = \tau_{rz} = 0 \qquad \text{at} \qquad z = \pm L$$

Here P_i and P_o are the inside and outside pressures and R_i and R_o are the inside and outside radii, respectively.

The solution $u(r,z)$, $W(r,z)$ of the equations (17), (18) can be made to depend on the solutions of two simpler problems:

Problem "A"

Solve the equations (17) in an infinitely long cylinder with the boundary conditions $\sigma_r = P_i,\ \tau_{rz} = 0$ at $r = R_i$ (19.1)

$$\sigma_r = P_o, \ \tau_{rz} = 0 \quad \text{at } r = R_o \tag{19.2}$$

and subject to the restriction that $\int_{R_i}^{R_o} \sigma_z r dr = 0$ (19.3)

Denote the displacements and stresses obtained by the subscript "A", i.e. u_A, W_A, σ_{r_A}, etc.

Problem "B"

Solve the equations (17), without the thermal stress terms which appear on the right hand side of (17.1), in a semi-infinite cylinder with the boundary conditions $\sigma_r = \tau_{rz} = 0$ at $r = R_i$ (20.1)

$$\sigma_r = \tau_{rz} = 0 \quad \text{at} \quad r = R_o \tag{20.2}$$

$$\sigma_z = F(r), \ \tau_{rz} = G(r) \text{ at } z = 0 \tag{20.3}$$

The function $F(r)$, which gives the distribution of normal forces over the end of the cylinder, is subject to the condition that

$\int_{R_i}^{R_o} F(r)\, r dr = 0$, i.e. these forces must (20.4)

be self-equilibrating. In obtaining the stresses σ_θ, σ_r, σ_z, τ_{rz} omit the thermal stress terms $B_1(T)$, $B_2(T)$ in (16.1), (16.2), (16.3). Denote the displacements and stresses obtained by the subscript "B".

If both problems "A" and "B" have been solved, the solution u, W of the original problem (17), (18) may be obtained as follows:

Apply the formulae for problem "B" with $F(r) = -\sigma_{z_A}$, $G(r) = 0$. Call the resulting displacements and stresses ${}^1u_B$, ${}^1W_B$, ${}^1\sigma_{r_B}$, etc.

Apply the formulae for problem "B" with $F(r) = -\left[{}^1\sigma_{z_B}\right]_{z = 2L}$, $G(r) = -\left[{}^1\tau_{rz_B}\right]_{z = 2L}$. Call the resulting displacements and stresses ${}^2u_B$, ${}^2W_B$, ${}^2\sigma_{r_B}$, etc.

Apply the formulae for problem "B" with $F(r) = -\left[{}_2\sigma_{z_B}\right]_{z=2L}$, $G(r) = -\left[{}_2\tau_{rz_B}\right]_{z=2L}$. Call the resulting displacements and stresses ${}_3u_B$, ${}_3W_B$, ${}_3\sigma_{r_B}$, etc.

And so forth - - -

The solution of the original problem can now be written as

$$u = u_A(r) + {}_1u_B(r, L-z) + {}_2u_B(r, L-z) + \ldots + {}_1u_B(r, L+z) + {}_2u_B(r, L+z) + \qquad (21.1)$$

$$W = W_A(r_1z) + {}_1W_B(r, L-Z) + {}_2W_B(r, L-z) + \ldots + {}_1W_B(r, L+z) + {}_2W_B(r, L+z) + \ldots \qquad (21.2)$$

$$\sigma_r = \sigma_{r_A}(r) + {}_1\sigma_{r_B}(r, L-z) + {}_2\sigma_{r_B}(r, L-z) + \ldots + {}_1\sigma_{r_B}(r, L+z) + {}_2\sigma_{r_B}(r, L+z) + \ldots \qquad (21.3)$$

and so forth .....

The series (21) should converge rapidly if the ratio $\frac{R_o-R_i}{L}$ of the cylinder wall thickness to the cylinder half-length is small.

A similar image superposition procedure will reduce any problem involving single or composite elastic solids of revolution to a problem of type "A", dealing with the response of an infinite solid to pressurization and thermal stresses, and problems of type "B", dealing with the response of a semi-infinite solid to self-equilibriating normal stresses and tractions applied to the end surface.

It should be noted that the equations (17) can be used to calculate transient thermal stresses only if the elastic constants

C_{11}, C_{12}, C_{13}, C_{22}, C_{44} are independent of temperature for the temperature range being considered. If this is not the case, additional terms appear in the equations (17). The reduction to problems of the types "A" and "B" can still be carried out, but the type "B" equations are no longer free of thermal stress terms.

We will now consider the problem "A" for a hollow cylinder of transversely isotropic material, making the assumption that the elastic constants are independent of temperature:

Since the cylinder is infinitely long,

$$\frac{\partial \sigma_r}{\partial z} = \frac{\partial \sigma_\theta}{\partial z} = \frac{\partial \sigma_z}{\partial z} = 0, \ \tau_{rz} = \gamma_{rz} = 0, \text{ and } \frac{\partial \epsilon_r}{\partial z} = \frac{\partial \epsilon_\theta}{\partial z} = \frac{\partial u}{\partial z} = 0.$$

Moreover, the cylinder is in a state of constant axial strain; i.e. $\epsilon_z = \frac{\partial W}{\partial z} = K$ (a constant), and $\frac{\partial W}{\partial r} = 0$. (These results hold for multi-layer, composite cylinders also.)

The second equilibrium equation (17.2) is satisfied identically. The first equilibrium equation (17.1) reduces to

$$\frac{d^2u}{dr^2} + \frac{1}{r}\frac{du}{dr} - \frac{C_{11}}{C_{22}}\frac{u}{r^2} = \frac{B_2(r) - B_1(r) - K(C_{12} - C_{13})}{C_{22}r} + \frac{1}{C_{22}}\frac{dB_2}{dr} \qquad (22.1)$$

Using the relations (16), the boundary conditions (19.1), (19.2) reduce to

$$\sigma_r = C_{12}\frac{u}{R_i} + C_{22}\frac{du}{dr} + C_{12}K - B_2(R_i) = P_i \text{ at } r = R_i \qquad (22.2)$$

$$\sigma_r = C_{12}\frac{u}{R_o} + C_{22}\frac{du}{dr} + C_{12}K - B_2(R_o) = P_o \text{ at } r = R_o \qquad (22.3)$$

Finally, the condition (19.3) becomes

$$\int_{R_i}^{R_o} \sigma_z r dr = \int_{R_i}^{R_o} \left[C_{13} \frac{u}{r} + C_{12} \frac{du}{dr} + C_{11} K - B_1 (r) \right] r dr = 0 \quad (22.4)$$

This last condition (22.4) will determine the constant K. The general solution of the equation (22.1) is of the form

$$u = \frac{C_{13} - C_{12}}{C_{22} - C_{11}} Kr + A_1 r^{\gamma} + A_2 r^{-\gamma}$$
$$+ \frac{r^{\gamma}}{C_{22}} \int_{R_i}^{r} r^{-1-2\gamma} \int_{R_i}^{r} \left[\frac{R_2(r) - B_1(r)}{r} + \frac{dB_2}{dr} \right] r^{1+\gamma} \, drdr. \quad (23)$$

where A_1 and A_2 are arbitrary constants, and $\gamma = \frac{C_{11}}{C_{22}}$. (24)

We will consider only the case in which the cylinder is at a uniform temperature. The general solution of (22.1) is then

$$u = \frac{C_{13} - C_{12}}{C_{22} - C_{11}} Kv + \frac{B_2 - B_1}{C_{22} - C_{11}} r + A_1 r^{\gamma} + A_2 r^{-\gamma}. \quad (25)$$

When this expression is substituted into the boundary conditions (22.2), (22.3) and into the equilibrium condition (22.4), three simultaneous equations are found which must be solved for the three unknowns K, A_1, A_2. These equations may be written as

$$F_{11} K + F_{12} A_1 + F_{13} A_2 = G_1 \quad (26.1)$$

$$F_{21} K + F_{22} A_1 + F_{23} A_2 = G_2 \quad (26.2)$$

$$F_{31} K + F_{32} A_1 + F_{33} A_2 = G_3 \quad (26.3)$$

with

$$F_{11} = C_{12} + \frac{C_{13} - C_{12}}{C_{22} - C_{11}} (C_{12} + C_{22}) \quad (27.1)$$

$$F_{12} = (C_{12} + \gamma C_{22}) R_i^{\gamma - 1} \quad (27.2)$$

$$F_{13} = (C_{12} - \gamma C_{22})\, R_i^{-\gamma - 1} \tag{27.3}$$

$$G_1 = P_i + B_2 - \frac{C_{12} + C_{22}}{C_{22} - C_{11}} (B_2 - B_1) \tag{27.4}$$

$$F_{21} = C_{12} + \frac{C_{13} - C_{12}}{C_{22} - C_{11}} (C_{12} + C_{22}) \tag{27.5}$$

$$F_{22} = (C_{12} + \gamma C_{22})\, R_o^{\gamma - 1} \tag{27.6}$$

$$F_{23} = (C_{12} - \gamma C_{22})\, R_o^{-\gamma - 1} \tag{27.7}$$

$$G_2 = P_o + B_2 - \frac{C_{12} + C_{22}}{C_{22} - C_{11}} (B_2 - B_1) \tag{27.8}$$

$$F_{31} = \left(\frac{C_{13}^2 - C_{12}^2}{C_{22} - C_{11}} + C_{11} \right) \frac{R_o^2 - R_i^2}{2} \tag{27.9}$$

$$F_{32} = (C_{13} + \gamma C_{12}) \quad \frac{R_o^{1 + \gamma} - R_i^{1 + \gamma}}{1 + \gamma} \tag{27.10}$$

$$F_{33} = (C_{13} - \gamma C_{12}) \frac{R_o^{1 - \gamma} - R_i^{1 - \gamma}}{1 - \gamma} \tag{27.11}$$

$$G_3 = \left[B_1 - \frac{C_{12} + C_{13}}{C_{22} - C_{11}} (B_2 - B_1) \right] \frac{R_o^2 - R_i^2}{2} \tag{27.12}$$

Substitution of the solutions K, A_1, A_2 of the equations (26) into (25) gives the final expression for the radial displacement u. The stresses in the cylinder can then be found from the equations (16):

$$\sigma_r = F_{11}K + P_i - G_1 + (C_{12} + \gamma C_{22})\, A_1 r^{\gamma - 1} + (C_{12} - \gamma C_{22})\, A_2 r^{-\gamma - 1} \tag{28}$$

$$\sigma_\theta = F_{11}K + P_i - G_1 + (C_{11} + \gamma C_{12})\, A_1 r^{\gamma - 1} + (C_{11} - \gamma C_{12})\, A_2 r^{-\gamma - 1} \tag{29}$$

$$\sigma_z = \frac{2}{R_o^2 - R_i^2} (F_{31}K - G_3) + (C_{13} + \gamma C_{12})\, A_1 r^{\gamma - 1} + (C_{13} - \gamma C_{12})\, A_2 r^{-\gamma - 1} \tag{30}$$

The stresses in a cylinder of finite length will consist of "Problem A" stresses in the center such as those calculated from equations (28), (29), and (30), plus the additional stresses of the "Problem B" type near the ends of the cylinder. In particular, the shearing stress τ_{rz} is zero in the center portion of such a cylinder, but may become quite large near the cylinder ends. This fact has led to the conclusion that pyrolytic graphite coatings may fail near their edges. However, the quantitative evaluation of this effect depends on the development of methods for the solution of problems of the type "B", which are mathematically more difficult than those of type "A". Several approaches to these problems are being considered; details will be given in a later report.

V. MOTOR FIRING TESTS

Results were reported previously[1] for two pyrolytic graphite coatings of fine-grained microstructure. During the current quarter, a nozzle of coarse-grained microstructure was tested. The coarse material performed only slightly less favorably than the fine material. An average erosion rate of 0.16 mil/sec was observed during the 62-second firing at 917 psia average pressure. The test was made using Arcite 373 (aluminized, 5600°F flame temperature) and the segmented nozzle as in earlier tests. Figure 1 shows a section of the pyrolytic graphite coating before and after firing.

These data indicate that, even though a fine-grained microstructure is superior, a coarse microstructure can perform well in this propellant if the coating is free of major cracks and delaminations. Hotter-propellant firings are needed to critically differentiate between pyrolytic graphite coatings. Pyrolytic graphite can contribute to a real improvement in rocket nozzle technology in these hotter propellants.

The segmented test nozzle used in the Arcite 373 (5600°F) firings was modified for use with 6500°F Arcocel propellant. The throat section coated with pyrolytic graphite was lengthened to 3/4-inch and contoured to the standard nozzle configuration. A throat section of pyrolytic graphite was necessary because no other grade of graphite is available which will not erode excessively near the throat at these higher temperatures.

One nozzle test piece was coated for the contoured assembly, but a mechanical failure occurred in the substrate coincident with the furnace-tube failure. Since microscopic examination showed a void-free coating of fine-grained microstructure, process conditions will be duplicated for the next nozzle test section.

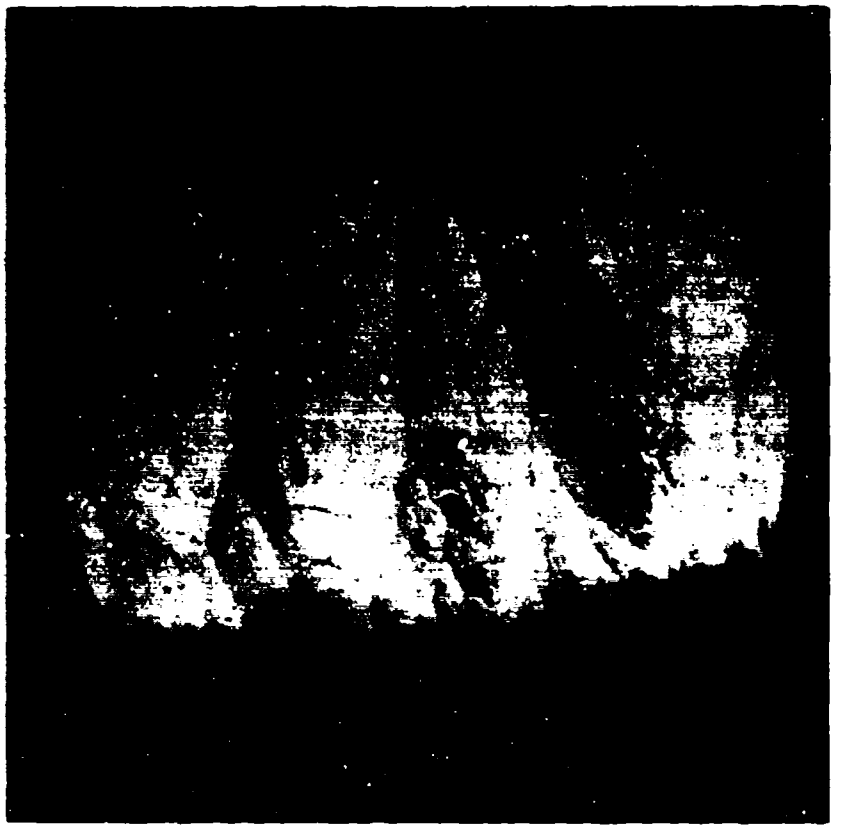

BEFORE

AFTER

Figure 1. Nozzle Coated with Coarse Grained Microstructure Pyrolytic Graphite Before and After Firing (185X)

VI. LITERATURE CITATIONS

1. Atlantic Research Corporation, "Improvement of Pyrolytic Graphite for Rocket Motor Applications," First Annual Summary Technical Report, Contract DA-36-034-ORD-3279 RD, July, 1961.

2. Love, "A Treatise on the Mathematical Theory of Elasticity" 4th Edition, pp. 152-156, Dover Publications, New York, 1944.

3. Timoshenko and Goodier, "Theory of Elasticity" 2nd Edition, p 3, The Maple Press Company, York, Pa., 1951.